Project Proposal

Semantic segmentation: a comparison between traditional and deep machine learning approaches in the multi-mineral classification of microscopy rock images.

David Bloomer
MSc Data Science
2018-2020

Supervisor: David Weston
Birkbeck College, University of London

Word Count (ex. Figures): 2950

Table of Contents

1. Abstract

This project aims to compare supervised machine learning approaches for multi-mineral classification through use of polarized-light microscopy rock images. Traditional approaches (support vector, random forest, gradient boosting, multilayer perceptron) will be compared against a state of the art fully convolutional network using data augmentation, to assess comparative performance and the potential to improve upon issues with model generality described within literature. The dataset comprises microscopy and quantitative mineralogy images from four Apollo 15 basalt samples. The optimal approach will be developed into a web application, with focus on both image classification and practical analytical interpretation.

2. Introduction

2.1 Project Objectives

This project aims to compare supervised machine learning approaches for use in multi-mineral classification of polarized-light microscopy digital rock image data. The project outcome will:

- Evaluate the suitability of machine learning approaches based on assessment of data requirements, computational efficiency, performance metrics, generality and probabilistic determination
- Identify the importance of image derived features in mineral classification
- Demonstrate capability for an end user application, analysing digital images interactively, with focus on both image classification and analytical interpretation (eg. rock classification)

2.2 Technical Outline

The project objective will be met by implementing several machine learning approaches for semantic segmentation – image classification at the pixel level. Literature cites test accuracy of up to 93.81% (Izadi et al., 2017) through traditional machine learning approaches for multi-mineral classification, yet sensitivity to image processing, image quality and a lack of generality are often attributed to reduced performance (Li et al., 2017). Use of a deep learning approach offers the potential to mitigate for these issues, and to the best knowledge of the author, have not been attempted to classify mineralogy using polarized-light microscopy data.

There is a strong focus on data preparation and feature engineering (Figure 1). Two parallel workflows will be considered, playing to the strengths of traditional and deep learning. For traditional learning, image properties will be standardised prior to training and a suite of feature engineering technique explored. For deep learning, data augmentation will be performed to improve generality, as features are learned to consider both variability in mineralogical and imaging. The study is not focused on defining deep learning architectures and will employ an existing solution proposed for multi-mineral classification of x-ray computed tomography (micro-CT) data.

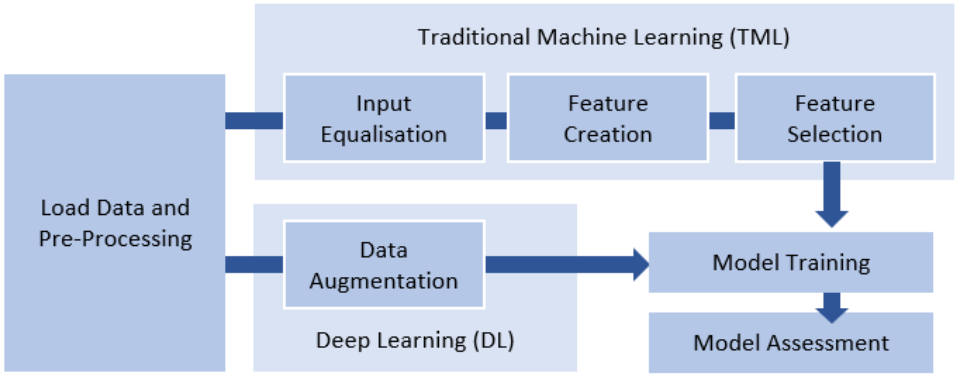

Figure 1. Data processing flow chart for traditional and deep learning workflows.

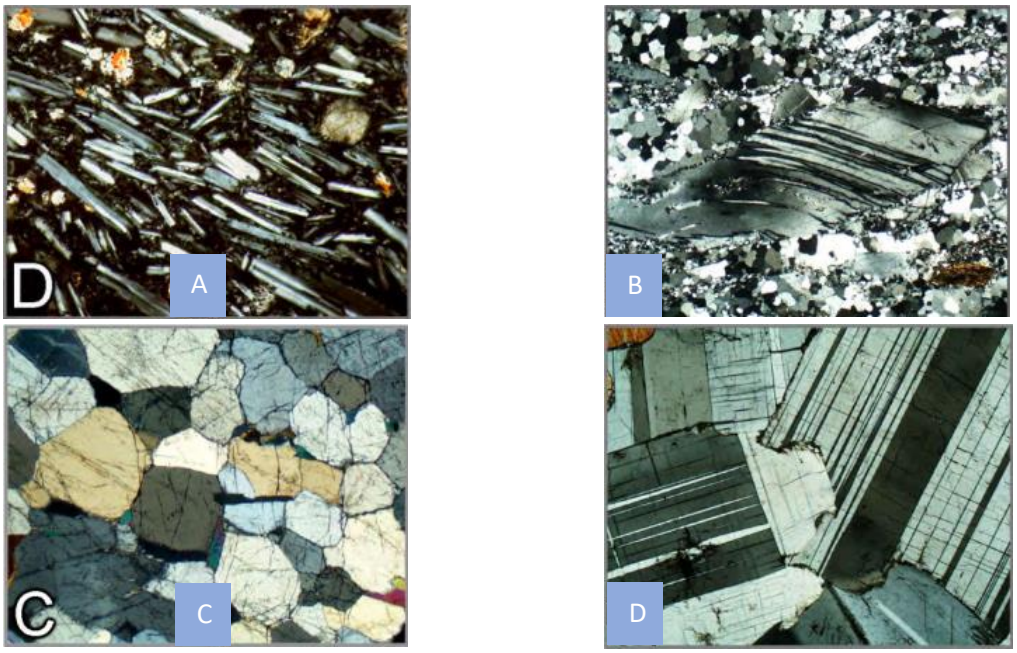

Figure 2: Example of single mineral, Feldspar, represented within plain polarized-light microscopy images, demonstrating variability in colour and texture: A. Basalt; B. Deformation and twinning; C. Recrystallisation; D. Polysynthetic twinning. Raith et al. (2012).

2.3 Project Data

Analysis of mineral composition provides key insights to a rock's chemistry, physical response and evolution. Minerals possess highly variable optical and morphological properties, in response to changes in phase and structure (Nesse, 2004) (Figure 2).

The dataset comprises polarized-light microscopy and quantitative mineralogy digital images from four Apollo 15 basalt samples. Sample mineralogy is typical of lunar basalts, being predominantly composed of pyroxene, plagioclase feldspar and olivine. Plain (PPL) and crossed polarized-light (XPL) microscopy images are provided by the School of Earth and Environmental Sciences at the University of Manchester. Quantitative mineralogy (QEMSCAN) images are released under Creative Commons 4.0 licensing through Mendeley Data. Details of the data collection methodology are outlined in Bell et al. (2020). A summary of mineral classes, proportions and image properties are given in Table 1.

A dataset containing scanning electron microscope (SEM) derived quantitative mineralogy interpretation data has been chosen for use in sample validation over manual segmentation to minimise interpretation bias.

PPL and XPL microscopy images are available as overlapping tiles, with QEMSCAN data as full sample images at 10 microns per pixel resolution. A significant amount of image processing is required to prepare data for machine learning ingestion. Based on an estimated sample image coverage of 60%, the processed dataset contains 70 million samples (pixels).

Sample	Split	Mineral Classes and Proportions (>1%)	Image Properties *n, pixels (format)*
15125	6	Matrix (51.4%), Pyroxene (45.3%), Olivine (3.1%)	PPL/XPL: 4, 1920x2560 (tif) QEMSCAN: 1, 3963 x 3567 (tif)
15475	15	Pyroxene (59.7%), Plagioclase Feldspar (30.2%)	PPL/XPL: 10, 1920x2560 (tif) QEMSCAN: 1, 4694 x 4717 (tif)
15555	209	Pyroxene (52.4%), Plagioclase Feldspar (30.4%), Olivine (12.1%)	PPL/XPL: 12, 1920x2560 (tif) QEMSCAN: 1, 6332 x 7077 (tif)
15597	18	Pyroxene (59%), Matrix (35%)	PPL/XPL: 4, 1920x2560 (tif) QEMSCAN: 1, 3998 x 4378 (tif)

Table 1: Technical summary of Apollo 15 basalt sample dataset comprising plain (PPL), crossed polarized-light (XPL) microscopy and quantitative mineralogy (QEMSCAN) images. Mineral proportions after Grove and Walker (1977), Schnare et al. (2008), Longhi et al. (1972), Weigand and Hollister (1973).

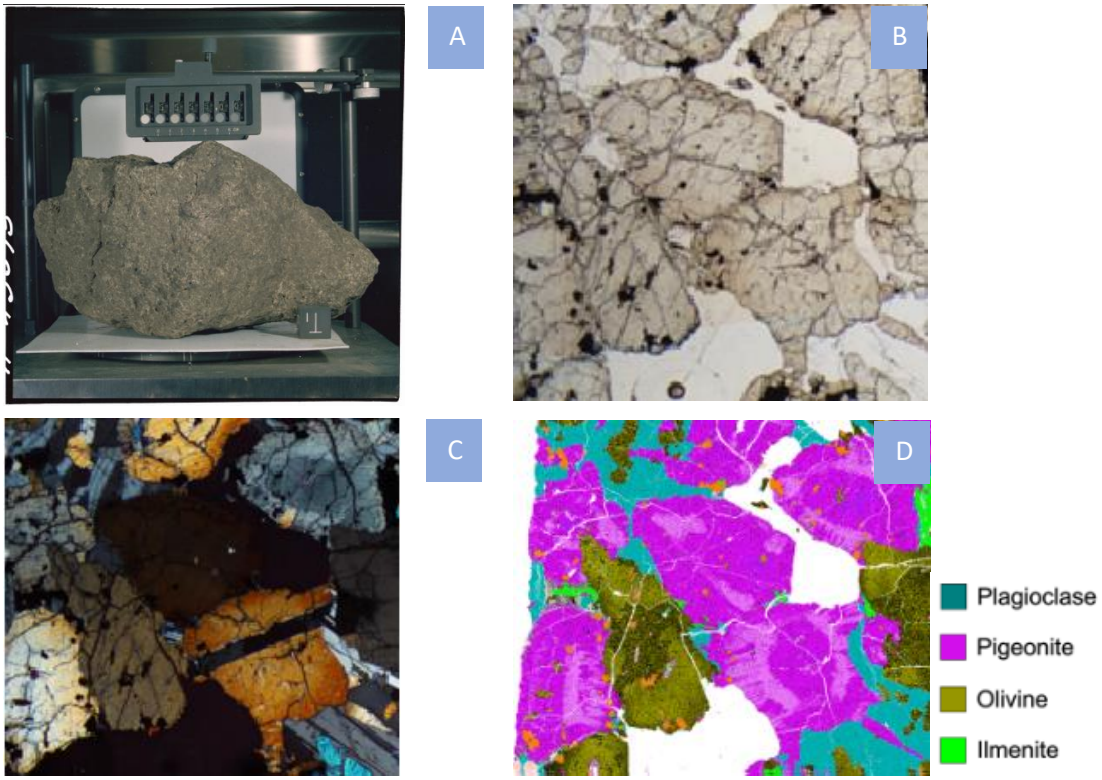

Figure 3: Apollo 15 Sample 15555 ("Great Scott") images, Split 209, Olivine basalt: A. Laboratory sample (LPI Lunar Sample Atlas, 2020); B. Plain polarized-light microscopy (5x magnification); C. Cross polarized-light microscopy (5x magnification); D. Quantitative mineralogy (QEMSCAN) (Bell et al., 2020). Note: Pigeonite is mineral in the Pyroxene group.

3. Literature Review

Literature describes various machine learning approaches to analyse specific aspects of a rock's composition and texture, to achieve grain-size, rock, rock cycle class, binary (grain-porosity) or multi-mineral classification. Classification is most typically performed using photographic, microscopy or micro-CT data sources. While textural classification of basalts has been performed (Singh et al., 2009), multi-mineral classification is most frequency performed for sedimentary rocks.

3.1 Image Processing

Image pre-processing is identified as a critical stage in determining model performance (Izadi et al, 2017). Potential issues can be broadly subdivided in to:

- Availability of labelled data
- Conditioning and standardisation of image quality
- Pixelwise registration between training data and labels
- Colour representation models

Quantitative mineralogy data is costly and time consuming to produce, and is therefore often sparingly collected to supplement microscopy data (Raith et al., 2012). This creates issues in terms of data availability, as semantic segmentation datasets for deep learning frequently surpass the billion-pixel mark (Wang et al., 2000).

Variation in image colour and texture, not caused by optical mineral properties, can be introduced through photographic equipment and technique. Standardised approaches to data collection have been proposed (Berrezueta et al, 2019), but are not common practise. To address image quality or variability, authors have performed filtering (Marmo et al., 2005; Singh et al., 2009; Izadi et al, 2017; Boyne, 2019), histogram equation (Dunlop, 2006), and normalisation of brightness or contrast (Izadi et al, 2017; Maitre et al, 2019; Rubo et al., 2019). Li et al. (2017) proposing a feature-based transfer learning approach to mitigate mineralogical and imaging variation between regions.

Data augmentation has been shown to increase the efficiency of small datasets (Garcia-Garcia et al., 2017), either increasing convergence or acting as a regularizer to increase potential for generalisation (Wong et al., 2016). Karimpouli and Tahmasebi (2019) proposed use of a cross-correlation simulation data augmentation approach for use with geological data.

Multiple authors conclude that pixelwise misalignment between input data and labels negatively impacts model accuracy (Maitre et al., 2019; Wang et al., 2000).

Colour representation is shown to have an impact in multiple studies. Authors cite an increase in performance using greyscale intensity, HSV (Thompson et al., 2001; Rubo et al, 2019) and CIELAB (Dunlop, 2006; Maitre et al., 1999) colour models respectively. While the RGB colour model is sensitive to fluctuations of the light source, HSV through hue describes colour by wavelength as perceived by humans (Thompson et al., 2001). CIELAB represents colour linearly, more closely approximating human colour perception (Fairchild, 2003).

3.2 Feature Engineering

A wide variety of features have been considered for use in edge and texture classification, with use of textural over colour features demonstrated to improve model generalisation (Guntoro et al., 2019). Approaches can be broadly classified in to filter bank, ridge, and Haralick categories.

Filter banks use arrays of filters to segment spatial frequency and directional characteristics of an image. The most common approach, a Gabor filter bank, performs a Fourier transform using a Gaussian function applied to the spatial and frequency domains (Clark et al., 1997). Ridge filters use eigenvalues of a Hessian matrix composed from second-order derivatives of image intensity to detect ridge, rather than edge, features within an image. Haralick filters are statistics derived from a gray level co-occurrence matrix (GLMC) (Haralick et al., 1973) describing patterns of repetition in greyscale intensity.

Jiang et al. (2018) demonstrated the potential to discriminate between mineralogy through variation in response to orientation and frequency Gabor filters. While Hessian ridge filters are cited as having a high feature importance for textural feature extraction (Peña et al., 2019; Rubo et al., 2019).

3.3 Traditional Machine Learning

Multi-mineral semantic segmentation of microscopy data been demonstrated through clustering (Guntoro et al., 2019), decision trees (Maitre et al., 2019), random forests (Maitre et al., 2019, Peña et al., 2019, Rubo et al., 2019) and multilayer perceptrons (MLP) (Thompson et al., 2001; Baykan and Yilmaz, 2010; Izadi et al, 2017; Rubo et al., 2019). Model performance varies significantly based on the learning approach and features selected, with further variability observed between class performance due to a dependency in classification on unique optical mineral properties.

Peña et al. (2019) and Rubo et al. (2019) have made comparisons between specific traditional machine learning approaches, both concluding that random forests have comparable performance metrics to MLPs at significantly reduced training times. Both single- and two- hidden-layer MLPs are considered as traditional machine learning approaches on the basis that feature creation is manually performed within literature.

3.4 Deep Machine Learning

Fully convolutional networks (Long et al., 2014) represent the current state of the art approach to semantic segmentation. The concept builds upon convolutional neural networks (LeCun et al., 1998), which exploit spatial correlation to characterise images through sets of learnable filters – convolution and pooling layers. The first layer extracts edge-like features and can be thought of as a filter bank approach, with subsequent layers increasing in complexity (Andrearczyk and Whelan, 2016).

In SegNet (Badrinarayanan et al., 2015), connected layers are replaced by convolution layers to create an encoder-decoder architecture, where low resolution feature maps are decoded back to full image dimensions, and classified through a softmax layer. U-Net (Ronneberger et al., 2015) modifies SegNet through addition of symmetrical concatenations between equivalent encoder-decoders to retain geometric information from initial layers and increase resolution. An alternate approach is ResNet (He et al., 2016), where a repeated encoder architecture is connected by skip connections, to improving training speed and scalability.

Fully convolution networks have been used on micro-CT imaging to classify mineralogy, utilising SegNet (Karimpouli and Tahmasebi, 2019), U-Net and ResNet architectures (Wang et al., 2020). Additionally, Wang et al. (2000) proposed the U-ResNet architecture, to combine the advantages of both approaches, producing a multi-mineral classification accuracy of 94.5%.

Limitations exist in terms of the types of features that fully convolutional networks can learn, with attempts made to integrate convolutional neural networks with Haralick features (Hu and Zheng, 2019).

3.5 Summary

Deep learning approaches offer the potential to improve generality, compensating for unsampled variation in mineralogy and imaging. While this projects dataset is relatively small at 90 million samples (2.3), data augmentation techniques are demonstrated to improve dataset efficiency.

The range of models explored for microscopy data in literature is limited, with no consideration of support vector or gradient boosting machines, which have proved to be highly successful for classification problems (Chen and Guestrin, 2016). This project will expand the range of machine learning approaches and features explored, selecting additional features from classes identified to be successfully in discriminating mineralogy.

4. Method

4.1 Data Preparation

To prepare data for ingestion within traditional machine learning, PPL and XPL microscopy images require stitching and then pixelwise registration with QEMSCAN data. Image stitching will follow the methodology proposed by Brown and Lowe (2007) due to its insensitivity to differences in order, orientation, scale and illumination. Alignment be performed through application of an Affine homography matrix calculated through random sample consensus (RANSAC) (Fischler and Bolles, 1981), matching feature vectors through a scale invariant feature transform. Features detected through SURF (Bay et al., 2008) are observed to provide sparsely populated features (Guntoro et al, 2019), so alternate techniques such as BRISK (Liu et al., 2018) will be explored to improve lateral pixelwise registration introduced by image distortion.

A data augmentation approach is required for deep learning to expand the number of samples and introduce variability into the dataset. The data augmentation workflow will include the following steps (simulating variation in):

- Affine Transformations (microscopic edge distortion)
- Rotation (texture orientation)
- Crop (image size)
- Scaling (image resolution)
- Noise (image quality)
- Blur (image quality)
- Colour variation though equalisation, brightness and contrast (imaging)

Where possible, data augmentation will be performed in-place using the python keras ImageDataGenerator class to reduce memory overhead and storage requirements.

4.2 Standardisation and Feature Engineering

A range of transformations and features have been chosen to discriminate colour, shape and texture attributes, based on those explored within literature. These both overlap and extend beyond those attainable through convolutional deep learning:

- Colour normalisation: equalisation, brightness and contrast
- Colour representation: HSV, CIELAB colour models
- Edge filters: Canny, Sobel
- Filter banks: Hessian, Maximum Response (MR8), Membrane
- Ridge filters: Frangi, Hessian, Sato, Meijering
- Haralick filters: contrast, dissimilarity, homogeneity, ASM, energy, correlation

4.3 Model Evaluation

Machine learning approaches will be evaluated based on assessment of data requirements, computational efficiency, performance metrics, generality and probabilistic determination.

Model performance will be assessed using the Dice (F1) and Jackard similarity coefficients, as typically used in semantic segmentation to compensate for class imbalance in images. Accuracy per mineral class and accuracy weighted by mineral fraction are both commonly reported within literature and will be generated to permit comparison.

4.4 Traditional Machine Learning

Despite the goal of comparing machine learning approaches in parallel, an AutoML approach is not suitable due to limitations in supported classifiers and a lack of dependency between data conditioning, feature engineering and the train-test split. A custom pipeline will be built using python sklearn library to systematically assess and understand the interplay between feature selection through recursive feature elimination and chosen models, as summarised model evaluation metrics. Hyperparameter tuning of the best approaches will be performed using a Bayesian optimization strategy. The following learning methods will be considered:

- Kernel Support Vector Machine
- Random Forest
- Gradient Boosting Machine (XGBoost / lightgbm)

If transformation of the colour model from the initial RGB colour model is determined to have a positive influence on classification, the transformation will be applied to the deep learning input data.

A multilayer perception will be implemented through python tensorflow, following the textural network architecture of Izadi et al. (2017). The network contains two-hidden-layers, containing 40 and 10 neurons respectively based on 10 input features, and uses a sigmoid activation function.

Given data extent is limited, k-fold cross validation of k=5 will be used to determine the test-train split for all models.

4.5 Fully Convolutional Neural Network

A fully convolutional network will be implemented through python tensorflow, following the two-dimensional U-ResNet architecture of Wang et al. (2020). The model architecture (for three-dimensions) is summarised in Figure 4.

Figure 4: U-ResNet architecture shown in three-dimensional microtomography configuration, project implementation will be modified for two-dimensional microscopy images. Wang et al., 2020.

4.6 Web Application

Following analysis of the model performance metrics, an optimal workflow will be chosen and turned in to a piece of functional python code. Unit testing will be performed to ensure code stability.

To demonstrate the capability for an end user application, an interactive web application will be created using the python streamlit library. Given image classification is often not the end-goal for users, graphical analytical interpretations will be provided quantifying bulk composition, rock classification, grain-size distribution and elastic behaviour. While most analysis represents mixing of mineral fractions, textural analysis requires estimation of grain shape, which will be performed using MSLIC multi-dimensional clustering (Jiang et al., 2018) to ensure stability. The application should possess the following user functionality:

- Select input image file for classification: either default samples from training dataset or loading image from the local computer
- Save multi-mineral classification on local computer as image file
- View analytical interpretation(s) of multi-mineral classification

The application will be deployed to the internet through use of a Docker container deployed to the Google Cloud Platform. The proposed graphical user interface shown in Figure 5.

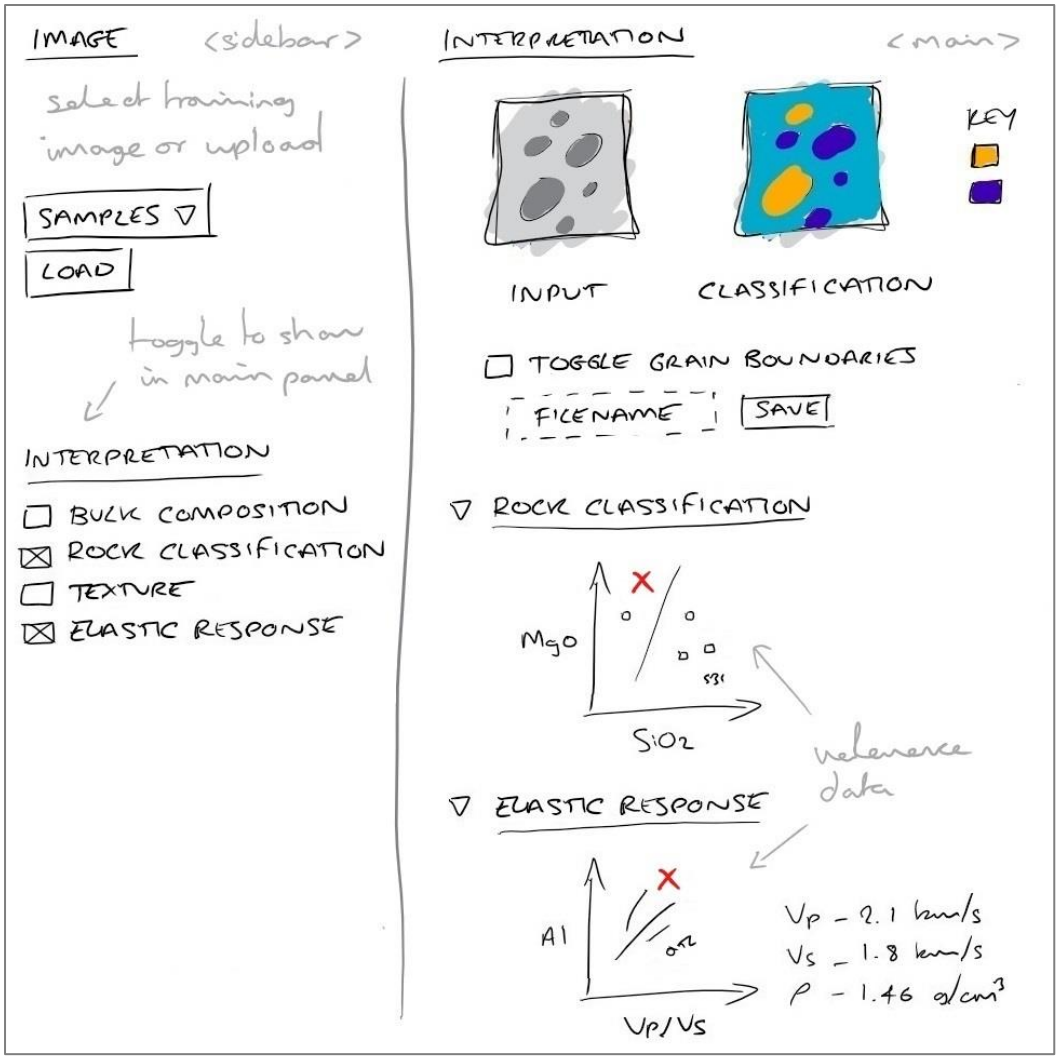

Figure 5: Web application graphical user interface. Based on python streamlit framework with organisation of contexts through main panel and user interface focused sidebar panel.

5. Tools and Software

Development will be performed using the python programming language, due to personal proficiency, and a strong user community allowing both integration of existing code through open source libraries, and outcomes of the project to be shared within the geoscience community.

Libraries

- numpy: support for multi-dimensional matrix data structure to represent images and features, underlying data structure for image processing libraries
- skikit-image: image processing, pre-processing and feature creation
- opencv: image processing, enhanced functionality for matrix warping
- skikit-learn: machine learning, support for feature selection, pipelining, classification algorithms (SVM, RandomForest) and performance metrics
- XGBoost: machine learning algorithm, gradient boosting classification
- lightgb: machine learning algorithm, gradient boosting classification
- hyperopt: hyperparameterisation – parameter tuning
- tensorflow (keras): machine learning library, implementation of multi-layer perceptron, fully convolutional neural network and performance metrics
- streamlit: web application framework
- conda: python environment and package management
- spyder: integrated development environment
- git: code and data version control
- pytest: testing

The following software applications are chosen to facilitate requirements outside of the python ecosystem:

Software as a Service (SaaS)

- GitHub: online private repository for redundancy

Platform as a Service (PaaS)

- Docker: containerisation of software to ease deployment
- Google Cloud Platform (GPC): application web hosting with academic account support

The final deliverable is a functional piece of python code. Deployment is not a strong focus for the project, given there is no target user base, and is performed for communication and demonstration purposes.

6. Project Planning

The machine learning development lifecycle is iterative by nature, creating the requirement for code (and data) version control through use of a private GitHub repository. Library version control through virtual environments is essential, given the code will ultimately be deployed.

To effectively manage the timeline of the project, consideration has been given to identify key risks associated with method, and a timeline created following a waterfall project management methodology (Figure 6).

6.1 Risk and Mitigation

The following risks have been identified, and are presented alongside efforts made to mitigate them:

- Dataset mineralogy: basalt mineralogy can contain complex colour and texture variation (Figure 2), literature demonstrates machine classification of only olivine for predominant minerals within the dataset
- Data availability: approximately 70 million data samples are available for training (2.3), representing a small proportion of those typically used in deep learning image datasets (3.1) – it is acknowledged that the dataset might not be suitable for deep learning, while data augmentation is attempted to increase dataset efficiency
- Computational resources: resources and training time for deep learning image projects can be significant – a desktop computer will be used for training, architecture of the fully convolutional network follows a published example to negate the need for iterative development, with implementation being frontloaded in the project timeline (6.2) to reduce potential for workflow dependencies

6.2 Timeline

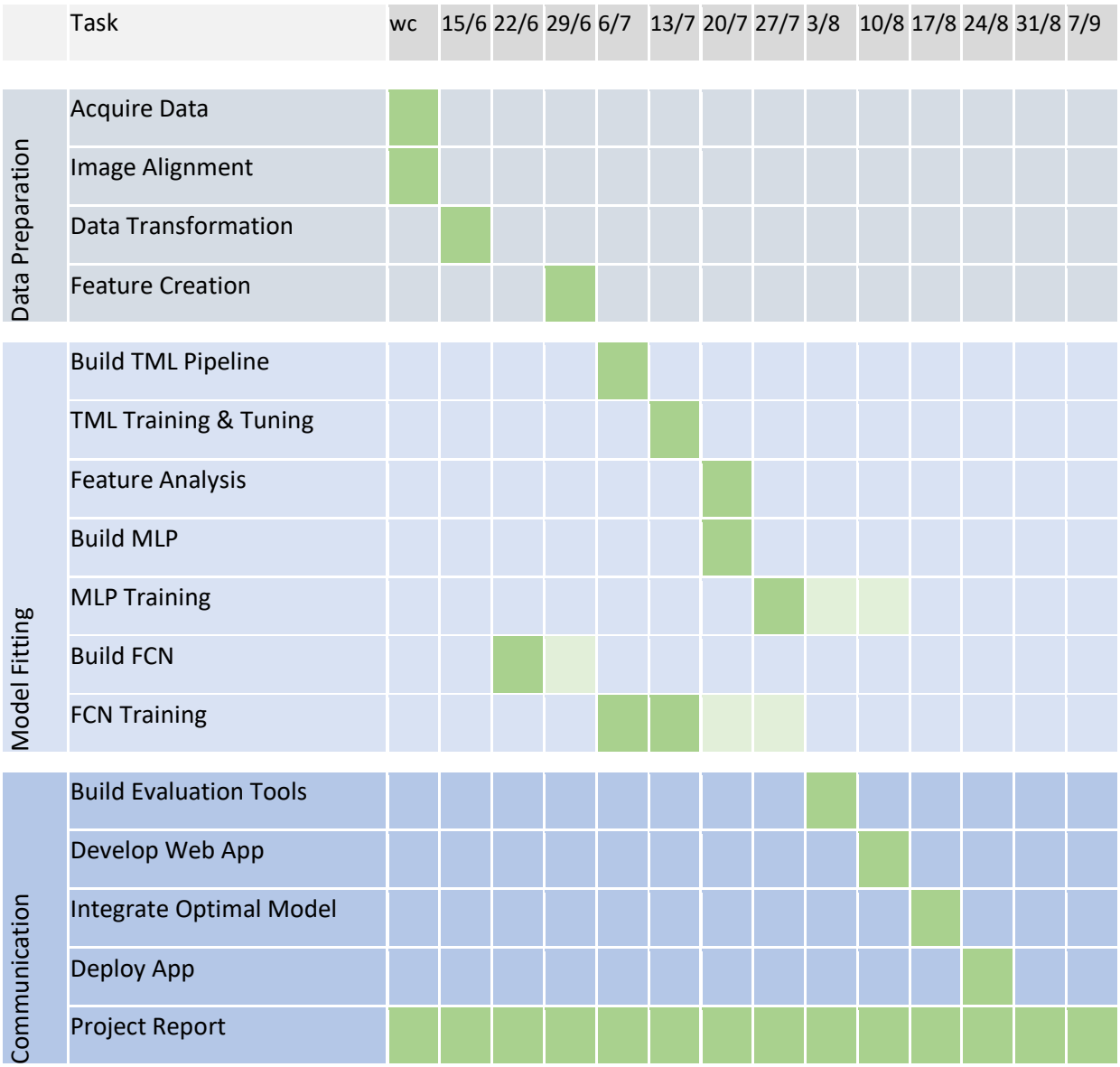

Figure 6: Project Timeline. Tasks are planned to take place during weeks highlighted in dark green. Contingency for critical phases is demonstrated in light green (6.1). Acronyms used: Week Commencing (wc). Traditional Machine Learning (TML). Multilayer Perceptron (MLP). Fully Convolutional Network (FCN).

7. References

7.1 Publications

Andrearczyk, V., Whelan, P. F., 2016, Using Filter Banks in Convolutional Neural Networks for Texture Classification, Pattern Recognition Letters, 84, 63–69.

Badrinarayanan, V., Kendall, A., Cipolla, R., 2015, Segnet: A deep convolutional encoder-decoder architecture for image segmentation, IEEE Transactions on Pattern Analysis and Machine Intelligence.

Bay, H., Ess, A., Tuytelaars, T. and Van Gool, L., 2008, Speeded-up robust features (SURF), *Computer vision and image understanding*, *110*, 346-359.

Baykan, N. A., Yilmaz, N., 2010, Mineral identification using color spaces and artificial neural networks, Computers and Geosciences, 36, 91-97.

Bell, S., Joy, K., Pernet-Fisher, J., Hartley, M., 2020, Data for: "QEMSCAN as a method of semi-automated crystal size distribution analysis: Insights from Apollo 15 mare basalts", Mendeley Data, v1.

Berrezueta. E., Domínguez-Cuesta, M. J., Rodríguez-Rey, Á, 2019, Semi-automated procedure of digitalization and study of rock thin section porosity applying optical image analysis tools, Computers and Geosciences, 124, 14-26.

Boyne, R. M. G., 2019, Automated Analysis of Thin Section Images, Master's thesis, Imperial College London.

Brown, M., Lowe, D. G., 2007, Automatic panoramic image stitching using invariant features, International journal of computer vision, 74, 59-73.

Chen, T., Guestrin, C., 2016, XGBoost: A Scalable Tree Boosting System, Proceedings of ACM SIGKDD International Conference on Knowledge Discovery and Data Mining, 785-794.

Clark, M., Bovik, A. C., Geisler, W. S., 1997, Texture segmentation using Gabor modulation/demodulation, Pattern Recognition Letters, 6, 261-267.

Dunlop, 2006, Automatic Rock Detection and Classification in Natural Scenes, Master's thesis, Carnegie Mellon University.

Fischler, M. A., Bolles, R. C., 1981, Random sample consensus: a paradigm for model fitting with applications to image analysis and automated cartography, *Communications of the ACM*, *24*, 381-395.

Garcia-Garcia, A., Orts-Escolano, S., Oprea, S. O., Villena-Martinez, W., Garcia-Rodriguez, J., 2017, A Review on Deep Learning Techniques Applied to Semantic Segmentation, ArXiv.

Grove, T. L., Walker, D., 1977, Cooling histories of Apollo 15 quartz-normative basalts, Proceedings 8th Lunar Science Conference, 2, 1501-1520.

Guntoro, P. I., Tiu, G., Ghorbani, Y., Lund, C., Rosenkranz, J., 2019, Application for machine learning techniques in mineral phase segmentation for X-ray microcomputed tomography (CT) data, Minerals Engineering, 142.

Haralick, R. M., Shanmugam, K., Dinstein, I., 1973, Textural Features for Image Classification, IEEE Transactions on Systems, Man and Cybernetics, 3, 610–622.

He, K., Zhang, X., Ren, S., Sun, J., 2016, Deep residual learning for image recognition, *Proceedings of the IEEE conference on computer vision and pattern recognition,* 770-778.

Hu, Y., Zheng, Y., 2019, A GLCM Embedded CNN Strategy for Computer-aided Diagnosis in Intracerebral Hemorrhage, ArXiv.

Izada, H., Sadri, J., Bayati, M., 2017, An intelligent system for mineral identification in thin sections based on a cascade approach, Computers and Geosciences, 99, 37-49.

Jiang, F., Gu, Q., Hao, H., Li, N., Wang, B., Hu, X., 2018. A method for automatic grain segmentation of multi-angle cross-polarized microscopic images of sandstone, *Computers and Geosciences*, *115*, 143-153.

Karimpouli, S., Tahmasebi, K., 2019, Segmentation of digital rock images using deep convolutional autoencoder networks, Computers and Geoscience, 126, 142-150.

LeCun, Y., Bottou, L., Bengio, Y., Haffner, P., 1998. Gradient-based learning applied to document recognition, IEEE, 86, 2278– 2324.

Li, N., Hao, H., Gu, Q., Wang, D., Hu, X., 2017, A transfer learning method for automatic identification of sandstone microscopic images, Computers and Geosciences, 103, 111-121.

Long, J., Shelhamer, E., Darrell, T., Fully convolutional networks for semantic segmentation, IEEE Computer Vision and Pattern Recognition, 3431–3440.

Longhi, J., Walker, D., Stolper, E. N., Grove, T. L., Hays, J.F., 1972, Petrology of mare/rille basalts 15555 and 15065, The Apollo 15 lunar samples, 131-134.

Maitre, J., Bouchard, K., Paul Bédard, L., 2019, Mineral grains recognition using computer vision and machine learning, Computers and Geosciences, 130, 84-93.

Marmo, R., Amodio, S., Tagliaferri, R., Ferreri, V., Longo, G., 2005, Textural identification of carbonate rocks by image processing and neural network: Methodology proposal and examples, Computing and Geoscience, 31, 649-659.

Marschallinger, R., 1997, Automatic Mineral Classification in the Macroscopic Scale, Computers and Geosciences, 23, 119-126.

Peña, A., Caja, M. Á., Campos, J. R., Santos, C., Pérez, J. L., Fernández, P. R., Tritlla, J., 2019, Application of Machine Learning models in thin sections image of drill cuttings: lithology classification and quantification (Algeria tight reservoirs), EAGE/ALNAFT Geoscience Workshop.

Ronneberger, O., Fischer, P., Brox, T., 2015, U-net: Convolutional networks for biomedical image segmentation, Proceedings of Conference on Medical image computing and computer-assisted intervention, 234-241.

Rubo, R. A., Carneiro, C., Michelon, M F., Gioria, R., 2019, Digital petrography: Mineralogy and porosity identification using machine learning algorithms in petrographic thin section images, Journal of Petroleum Science and Engineering, 183.

Schnare, D. W., Day, J. M. D., Norman, M. D., Liu, Y., Taylor, L. A., 2008, A laser-ablation ICP-MS study of Apollo 15 low-titanium olivine-normative and quartz-normative mare basalts, Geochimica et Cosmochimica Acta, 72, 2556-2572.

Singh, N., Singh, T. N., Tiwary, A., Sarkar, K. M., 2009, Textural identification of basaltic rock mass using image processing and neural network, Computers and Geosciences, 27, 301-310.

Thompson, S., Fueten, F., Bockus, D., 2001, Mineral identification using artificial neural networks and the rotating polarizer stage, Computer and Geosciences, 27, 1081-1089.

Wang, Y. D., Armstrong, R. T., Shabaninejad, M., Mostaghimi, P., 2020, Physical Accuracy of Deep Neural Networks for 2D and 3D Multi- Mineral Segmentation of Rock micro-CT Images, arXiv.

Weigand, P. W., Hollister, L. S., 1973, Basaltic vitrophyre 15597: An undifferentiated melt sample, Earth and Planetary Science Letters, 19, 61-74.

Wong, S. C., Gatt, A., Stamatescu, V., McDonnell, M. D., 2016, Understanding data augmentation for classification: when to warp?, Computer Vision and Pattern Recognition, arXiv.

7.2 Books

Fairchild, M. D., 2013, Color Appearance Models. John Wiley and Sons. 472 pp.

Nesse., W. D., 2004, Introduction to Optical Mineralogy, Third Edition. Oxford University Press. 348pp.

Raith, M. M., Raase, P., Reinhardt, J., 2012, Guide to Thin Section Microscopy, Second Edition. Open Access Publication. 127pp.

7.3 Internet

LPI Lunar Sample Atlas, https://www.lpi.usra.edu/lunar/samples/atlas/#Apollo%2015, accessed 17th April 2020.

Mendeley Data, https://data.mendeley.com/datasets/rh37cdm9hv/1, accessed 14th April 2020.

NASA Lunar Sample Compendium, https://curator.jsc.nasa.gov/lunar/lsc/index.cfm, accessed 17th April 2020.